Numerical Methods in Civil Engineering

Journal Homepage: https://nmce.kntu.ac.ir/

Numerical study on the influence of near-fault and far-fault earthquakes on a subway station with emphasis to scattering on the wave propagation

***Mohsen Isari*[*], *Kosar Hadidi* [**], *Seyyed Kazem Razavi* [***], *and Reza Tarinejad* [****]**

ARTICLE INFO

RESEARCH PAPER

Article history:
Received:
January 2023.
Revised:
May 2023.
Accepted:
May 2023.

Keywords:
Subway station,
Near-Fault and Far-Fault earthquakes,
Spectral ratio,
Scattering of the wave,
Nonlinear cyclic model

Abstract:

To improve the design of surface structures built on underground structures for safety and earthquake resistance, it is necessary to study the effects of the underground structures on wave propagation scattering and surface ground acceleration. To this end, various parameters must be studied, including input motion, structure embedment, and dimensions of different subway stations. The present study focuses on these parameters by employing a nonlinear cyclic model called ARCS soil's shear modulus reduction and damping ratio increase corresponding to those given by the user. The variations in spectral ratio, affected period range, peak ground acceleration, and peak relative lateral displacement versus relative distance under near-fault and far-fault earthquakes are presented. The results indicate that different amplification or de-amplification effects at different surface positions were produced at each frequency by appearing a significant influence on the dynamic behavior of ground surface, soil layers, and the surface structure when a subway station is present. A 1.3 times increase in the surface ground acceleration when subjected to far-fault earthquakes and a 1.6 times increase in the relative displacement indicated that study parameters have significant influence on the amplification ratio and scattering of wave.

1. Introduction

Subway is one of the vital transportation solutions in densely populated cities. Another aspect of the importance and sensitivity of the subway is its frequent construction in congested urban areas, passing through major financial and commercial centers, which influences the earthquake resistance of ground surface structures [1], [2], [3]. To reach their required safety, it is necessary to consider the effects of the underground structures on the scattering of the seismic wave and the surface ground acceleration based on the experience of some destructive earthquakes [4], [5], [6]. Some previous research studied the seismic response of subways and their interaction with topographic features and surface structures [7], [8], [4], [9], [10] conducted a parametric study on the Daikai subway station using two-dimensional modeling, focusing on the influence of the material properties. Their results indicated that the weight of the subway has an insignificant impact on the lateral relative deformation of the structure. Isari et al. [6] investigated the effects of uniform and non-uniform excitations on the seismic response of the underground structures and ground surface acceleration using the extended identification method. They showed the power of the identification method in obtaining the natural frequency and damping of subway structures.

Sun et al. [4] investigated the change of surface ground motion due to the presence of a subway station under vertically propagating seismic waves using numerical analyses. Their parametric study considered various dimensions of subway station and wave characteristics. They showed that a significant amplification and a horizontal peak ground acceleration appears at the edge of

* *Corresponding author: Assistant Professor, Department of Civil Engineering, Faculty of Engineering, University of Kurdistan, Sanandaj, Kurdistan, Iran. E-mail: m.isari@uok.ac.ir*
** *Graduate Student, Dept. of Geotechnical Engineering, Faculty of Civil Engineering, Univ. of Tabriz, Tabriz, Iran. Email: Kosar.Hadidi@yahoo.com*
*** *Ph.D. Student, Department of Civil, Geological and Mining Engineering, Polytechnique Montréal, Montréal, Quebec, Canada. ORCID: https:// orcid.org/0000-0002-1864-6884. Email:Seyyed-kazem.razavi@polymtl.ca, SKRazavi2010@gmail.com*
**** *Professor, Department of Civil Engineering, University of Tabriz, 29 Bahman Blvd. 51666-16471, Tabriz, Iran. E-mail: r_tarinejad@tabrizu.ac.ir*

https://doi.org/10.61186/NMCE.2302.1005

the larger subway station and in the vicinity of the Daikai station, respectively. Other researchers [11], [12], [13], [14], [15] used the boundary element method to study the ground surface displacement and dynamic behaviour of the underground structures. They concluded that the presence of underground cavities had a noteworthy effect on the amplification generated on the ground surface. Zhuang et al. [16] investigated the seismic performance and instability of shallow-buried underground structures using statistical numerical methods. Their results showed the impact of input ground motions on the IDA curves. In their study, a statistical method was developed and the seismic instability curves were compared with previous research outcomes. Zhu et al. [17] investigated the effect of nearby ground structures on the dynamic response of underground structures in saturated soil. They used a constitutive plasticity model to simulate the large post-liquefaction deformation behaviour of saturated sand. The results indicated a significant impact of nearby ground structures on the main underground structure's seismic response in saturated soil.

Ma et al. [18] improved the seismic performance of underground structures by employing a newly proposed mechanism called a shock-absorbing gap to simulate the connection between sidewalls and slabs. The numerical results indicated that the shock absorbing gap affects the response of structural members during earthquakes. Gao et al. [19] employed an extended response spectrum method for dynamic analysis of underground structures. Ding et al. [20] investigated the dynamic response of underground structures in coral sand by using a series of shaking table model tests on underground structures. Zhou et al. [21] investigated the dynamic response of underground structures subjected to ground motion using theoretical, experimental, and numerical methods. Zhu et al. [22] used various seismic response analysis methods for systematic evaluation of the underground structures in saturated sand.

The present study uses a nonlinear cyclic model called ARCS (Axis Rotation-Cubic Spline) to simulate the shear modulus reduction and damping ratio increase of soil corresponding to those given by the user. There are nonlinear cyclic models defined in FLAC to simulate the seismic behaviour of soil-type structures. These models are based on Masing rules, which forces the unloading/reloading path to follow the curve controlled by the shape of the backbone curve. As a result, soil damping is eliminated at low strains and predicted for at large strains. Regarding the dynamic properties of the soils, many researchers have worked on the estimation of the maximum shear modulus model (Wichtmann and Triantafyllidis, [23], Payan et al. [24], [25] The modulus reduction and damping curves have also been investigated for clay and soils by many researchers [26], [27], [28]. The ARCS is a novel nonlinear cyclic model introduced by Yniesta et al. [29] in which new rules were developed to overcome the mentioned shortcomings. This new model helps the users to employ any desired backbone and damping curve. Consequently, the damping and stress-strain behaviour of soils simulated according to the input curves. This model, used in this study, has been written in C++ language programming code, added into FLAC to improve the software.

The aim of the present study is to conduct a parametric investigation of impact of underground structures on scattering of wave propagation and surface ground acceleration, using ARCS model with 14 different models. The study will consider various factors such as subway geometry, including a range of spans in its cross-section (ranging from 1 to 3), and the structure's location, which will be examined in three different positions. Through this analysis, the study aims to address questions related to the effects of the mentioned parameters on the horizontal ground acceleration, peak relative lateral displacement, and PGA on the soil layers in the vicinity of both near-fault and far-fault earthquakes.

2. Numerical Modeling

The numerical modeling was performed using the finite difference-based, FLAC software. Figure 1 illustrates the soil layers along with meshing, the underground structure with two spans, and boundary conditions for the dynamic analysis. The properties of soil layers are summarized in Table 1. The geometry of the subway and soil layers is associated with the Daikai subway station in Japan (Xu et al. 2019). The length of the model was chosen to be sufficiently large (14 times the width of the subway) to accurately simulate wave propagation in the model, taking into account incoming waves from the source and the structure. To prevent reflection of waves from the boundaries, absorbing boundaries, were placed at the sides of the model. The distance between the ground surface and the top of the structure is z, which would take three different values, 4.8 m, 9.6 m, and 14.4 m. The first value of z corresponds to the depth of the Daiki subway, while the second and third values are obtained by doubling and tripling the depth of the Daiki subway, respectively. These specific values of z are practical and can be realistically implemented. Three different box-shaped structures with 1, 2, and 3 spans are considered for the underground structure, as shown in Figure 2. The middle columns have in a rectangular section with 1 m by 0.4 m in size. The central distance of middle columns from each other is 3.5 m. Lateral walls with the top and bottom slabs have an elastic modulus of 30 GPa with a density of 2500 kg/m3. For the middle columns, these values are divided by 3.5 m (the central distance of columns from each other) for use in two-dimensional numerical modeling.

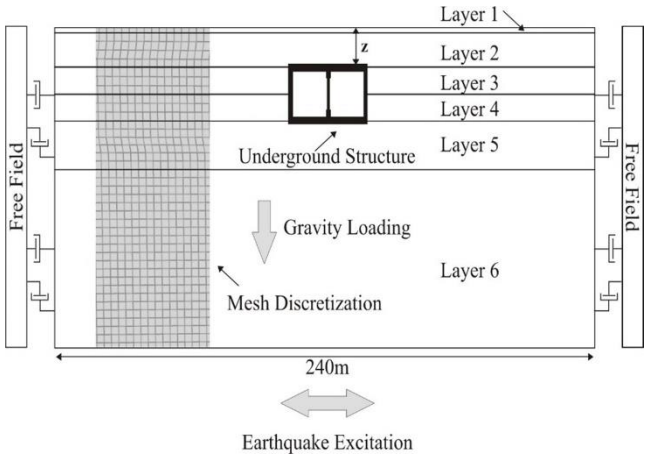

Fig. 1: Cross section of the two-span underground structure and the surrounding soil layers with free field boundary condition used in the dynamic simulation

To accurately simulate wave transmission through soil, the mesh size of the model for seismic analysis should be limited to 1/10 to 1/8 of the wavelength (λ_s) of the loading frequency [30]

$$Maximum\ Mesh\ Size = \frac{1}{8}\lambda_s = \frac{1}{8}\frac{V_s}{f_{max}} \quad (1)$$

where $f_{max}$is the highest frequency considered in the analysis and V_s is the shear wave velocity of the soil. Table 1 shows soil layer properties of soil type, layer properties including shear wave velocity, Poissons ratio, and unit weight. Taking into consideration the minimum V_s =140 m/s and f_{max} =15 Hz, the element size ranges between 0.93 m and 1.16 m [9]. Mesh discretization for some parts of soil layers is shown in figure 1.

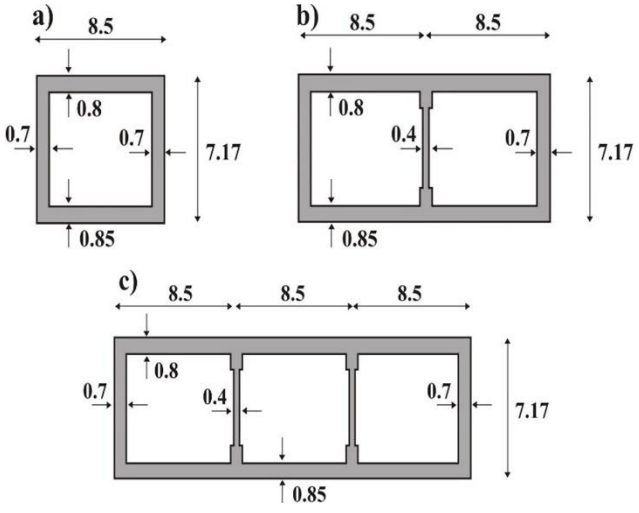

Fig. 2: Dimensions of underground structure (in meter) with (a) 1 span, (b) 2 spans, and (c) 3 spans

In the static analysis, roller and pinned supports were used for vertical boundaries and the bottom of the model, respectively.

Table 1: Physical properties of soils around the Daikai station [9]

	Type of Soil	Thickness (m)	Density (kg/m^3)	Shear Velocity (m/s)	Poisson's Ratio
Layer 1	Clay	1	19	140	0.333
Layer 2	Sand	4.1	19	140	0.488
Layer 3	Sand	3.2	19	170	0.493
Layer 4	Clay	3.1	19	190	0.494
Layer 5	Clay	5.8	19	240	0.490
Layer 6	Sand	22	20	330	0.487

The liner element in FLAC is used to model the structural components. The mechanical behavior of each liner element contains the structural response of the liner material itself and how the liner element interacts with the model mesh zones. Normal coupling spring properties control the normal direction of the liner-zone interface and shear coupling spring properties control the shear direction behaviour of the liner interface in terms of cohesive and frictional properties. Herein, the friction coefficient in the tangential direction is considered 0.4; while for the other direction, the separations between the soil and the structural elements are allowed. The damping ratio in these structural members is assumed to be 5%.

The static analysis employs the gravity loading technique with an elastic soil model to obtain the initial stress condition. In the dynamic analysis, it is better to use a nonlinear cyclic soil model to capture the hysteretic damping behavior of soils ([31], [9]). Nonlinear cyclic models need a maximum shear modulus at low shear strain (Gmax), the normalized modulus reduction curve, and a set of rules to define the unloading/reloading path. Depending on the rules, different seismic responses would be observed, which may overestimate or underestimate designing a structure. One of the famous ones is the Masing rules. In this case, the shape of the backbone curve controls the amount of damping produced by the soil during cyclic loading. In this technique, the calculated damping does not match the reality, resulting in a lower and over damping prediction in low and high cyclic shear strains, respectively (Yniesta et al. [29]). As a result, new rules need to overcome these problems. Yniesta et al. [29] have introduced a new set of rules that allow users to define the backbone curve and damping curve separately. Therefore, soil damping is simulated accurately at small and large strains according to the given damping curve. This feature is done by introducing the coordinate transformation technique in the shear stress-shear strain space. The horizontal axis of the new coordinate system (γ', τ') is from the reversal point (γ_L, τ_L) to the target reversal point (γ_R, τ_R). Reversal point is where change of loading happens. Target reversal point is determined based on the loading history. If the (γ_L, τ_L) is located on the backbone curve, the target reversal point is defined as $(\gamma_R = -\gamma_L, \tau_R = -\tau_L)$, (Figure 3a). Otherwise, the point gets the coordinates of the reversal point at the previous unloading/reloading path (Figure 3b).

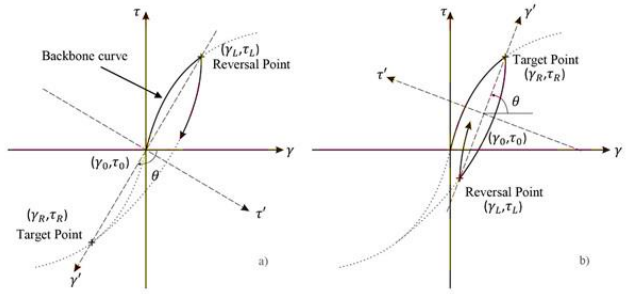

Fig. 3: Coordinate transformation based on the position of a reversal point situated (a) on the backbone curve or (b) on an unloading/reloading path (Yniesta et al. [29])

The direction of the τ' axis is controlled by the angle of rotation θ. The definition of θ ensures that the coming unloading/reloading path remains on the positive side of τ'(see figure 3). As a result, θ is defined by Eq. (2a) for loading in the -γ direction and Eq. (2b) for loading in the +γ direction.

$$\theta = tan^{-1}\frac{\tau_R - \tau_L}{\gamma_R - \gamma_L} - \pi \quad (2a)$$

$$\theta = tan^{-1}\frac{\tau_R - \tau_L}{\gamma_R - \gamma_L} \quad (2b)$$

The origin of this new space is also determined by the following equations ($\gamma_0 = \frac{\gamma_L+\gamma_R}{2}, \tau_0 = \frac{\tau_L+\tau_R}{2}$). It would be easy to define the unloading/reloading curve in the new coordinate system rather than in the original one. The ARCS model employs the following biquadratic equation.

$$\tau' = a\gamma'^4 + b\gamma'^2 + c \quad (3)$$

The parameters a, b and c are fitting parameters and are calculated to ensure that the area of the proposed curve in the transformed coordinate space matches a user-defined damping ratio.

$$a = \frac{5\pi D cos\theta(\tau_R - \tau_0)}{32{\gamma'_{in}}^4} \quad (4a)$$

$$b = -\frac{15\pi D cos\theta(\tau_R - \tau_0)}{16{\gamma'_{in}}^2} \quad (4b)$$

$$c = \frac{25\pi D cos\theta(\tau_R - \tau_0)}{32} \quad (4c)$$

where D is the damping ratio matches the cyclic shear strain from the damping curve, and γ'_{in} is calculated from following equation:

$$\gamma'_{in} = \frac{\gamma_R - \gamma_0}{cos\theta} \quad (5)$$

Using θ and the pair of (γ_0, τ_0) the values in the original system are related to those in the new system by Equation 6.

$$\begin{pmatrix}\gamma \\ \tau\end{pmatrix} = \begin{pmatrix}\gamma' cos\theta - \tau' sin\theta + \gamma_0 \\ \gamma' sin\theta + \tau' cos\theta + \tau_0\end{pmatrix} \quad (6)$$

The model employs the several other rules to follow the unloading/reloading paths using the coordinate transformation technique. It is encouraged that the reader refers to the paper (Yniesta et al. [29]) to see the complete definition of the model and the concept behind the rules. The ARCS model has been written in C++ code and added to FLAC to simulate the cyclic behaviour of the soils. For the present study, Gmax is calculated based on the elasticity theory and by using the shear wave velocity as follows:

$$G_{max} = \rho {V_s}^2 \quad (7)$$

Here, the curves were taken from Xu et al. [9] for clayey and sandy soil according to the graphs in Figure 4. As a verification, the model is subjected to the Kobe earthquake to see how the two spans of the underground structure respond to. The relative displacement of the top and bottom of the center column of the tunnel from the present study was compared with the results of Xu et al. (2019). According to the results shown in Figure 5, the maximum relative displacement from the present study, approximately 22 mm agrees well with the 20 mm displacement from Xu et al. [9].

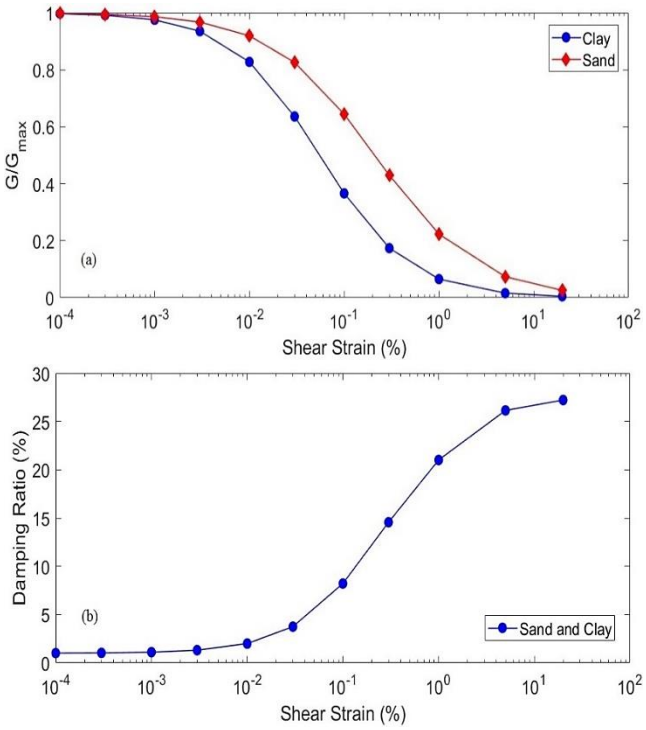

Fig. 4: (a) Normalized shear modulus reduction curve, (b) Damping curve (According to data of ([9])

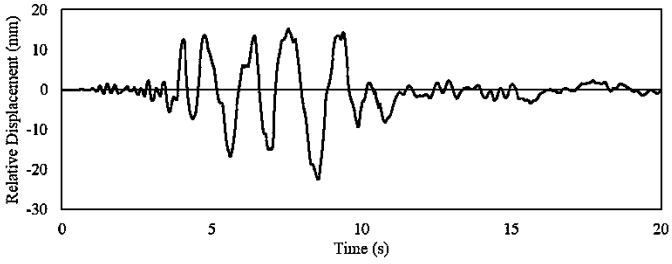

Fig. 5: Relative displacement between top and bottom of the center column in Daikai subway station

3. Near-fault and Far- fault earthquakes

Figure 6 shows two recorded earthquakes representing the near-fault and the far-fault ground motions characteristics (Table 2). The effect of these differences must be investigated in the dynamic responses of underground structures.

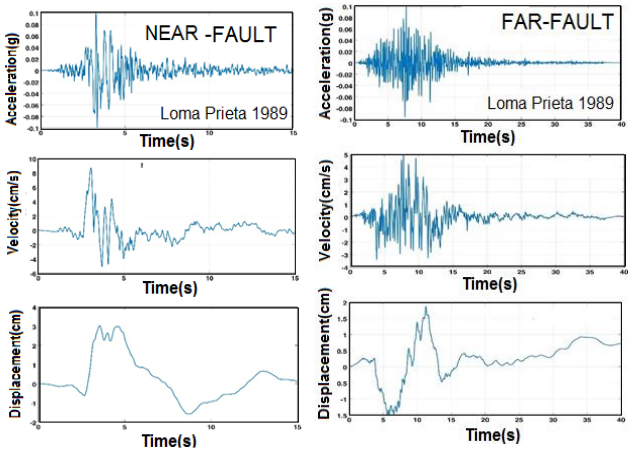

Fig. 6: Ground motions (acceleration, velocity, displacement) versus time plots of near-and far-fault earthquakes employed in the present study: 1989 Loma Prieta)

Table 2: Near-fault and far-fault earthquake records incorporated in the study.

Fault for ground motion	Earthquake name	Arias Intensity (m/s)	PGA (g)	PGV (cm/s)	Predominant Period (Tp)
Near-Fault	1989 Loma Prieta	0.07	0.1	8.66	0.4
Far-Fault	1989 Loma Prieta	0.12	0.1	4.95	0.16

4. Numerical models and observation points

The present paper performs a parametric study of a subway station to investigate the effect of its presence on the surface ground motion when the models are subjected to near-fault and far-fault earthquakes. To this end, a series of two-dimensional (14 models) numerical analyses accounting for various station dimensions (one span, two spans, three spans), the embedment of the structure (z1, z2, z3), and a free field model (without tunnel) were employed. Sixteen points on the ground surface, seven points on the soil layers, and two points on the structures were considered to investigate the possible amplification of the underground structure on the ground motions. Figure 7 indicates the position of the points specified for numerical analysis on the ground surface, between the soil layers and top and bottom on the underground structure.

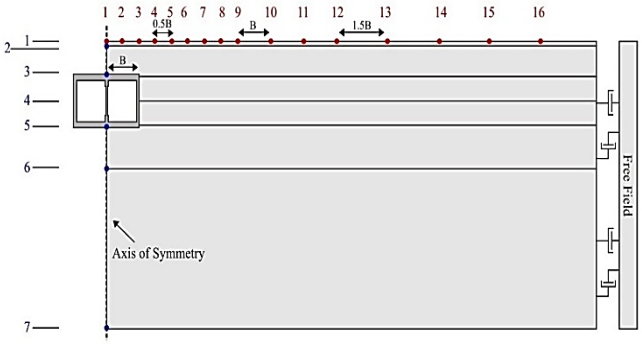

Fig. 7: Cross profile of Daikai station with the measurement points at different places

5. Effect of the near-fault ground motions

5.1 Effect of the cross-section dimension and embedment of the subway

Subways, if damaged or destroyed, may pose severe economic and fatal losses. Therefore, it is necessary to investigate the dynamic response of underground structures and their effects on the scattering on the wave and the surface ground acceleration. The impacts of underground structures have not been considered much attention from researchers on the seismic response of ground surface and possible magnification. Figure 8a illustrates the peak ground acceleration (PGA) on the ground surface versus the surface position in a preliminary free-field model (the model without the presence of the subway). Figures 8b, 8c, and 8d show the results for the role embedment of the subway station in the models. The presence of the subway station illustrates its significant role in the peak response, specifically near points 3, 4, 5, and 6, indicating that its effects cannot be ignored. As it seems, PGA in the free field model has similar values (2.2-2.3 m/s^2) at different surface positions. With the presence of the subway and its embedment increasing, first, the PGA on the ground surface decreases, and second, the time that scattered waves caused by the underground station that reaches the ground surface increases. The latter results in a reduction in the PGA of different surface positions. By increasing the subway cross-section dimension, the amplification/de-amplification effect is more evident at different points on the ground surface. The maximum PGA, occurring in the model with three spans at z1 level, is near 2.76 m/s^2, 1.25 times greater than the free-field site in the same surface position. Among the studied parameters in this section, the cross-section dimension of the subway has a higher impact than the embedment depth of the subway.

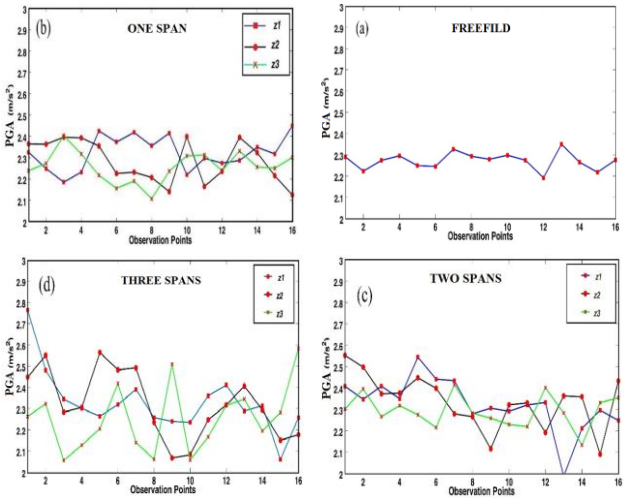

Fig. 8: Effect of the cross-section and embedment of the subway, a) free-field, b) one span, c) two spans, d) three spans, at different depths.

Figure 9 illustrates the PGA ratio (the PGA at the ground surface in the presence of a subway with two and three spans to the PGA at the same location for the subway with one span). The PGA ratio is high near the subway, reduces with increasing surface position distance from the subway. Increasing cross-section dimensions result in a higher PGA ratio ranging from 0.85 to 1.2. The maximum PGA ratio is 1.2 in the case of the three-span site analysis, which shows that the cross-section dimensions of the subway significantly affect the amplification of the PGA, where PGA amplification ratio will be smaller when the subway position becomes deeper. It also can be found that when the subway cross-section is increase, amplification or de-amplification effects at different surface positions are increased. The amplification or de-amplification effect is more significant when the surface positions are near to the subway.

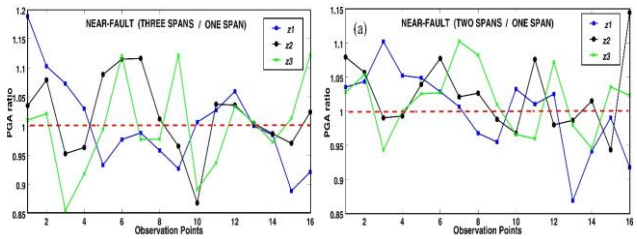

Fig. 9: Effect of station width on the surface ground motion, a) ratio of the PGA of the surface accelerations in the two-span to the one-span site, b) ratio of the PGA in the three-span to the one-span site.

5.2 Effect of the width and embedment of the station on soil layer position

This section provides a discussion regarding the effect of the subway station on PGA in soil layers. Figure 10 shows the PGA on the soil layers for the subways with different depth locations and sizes in cross-section. As seen in this figure, the PGA caused by the subway station cannot be disregarded. When the station embedment becomes deep, soil layers record lower PGA. At the position of 1 to 8, the PGA pattern affected by the station with two-spans and three-spans is very similar. At the position of 3 located exactly on the underground structure, the PGA amplification has experienced less response than the position of 4. This feature can be attributed to the fact that a "presence effect" caused by the subway station hindering this position from being directly affected by the upward seismic wave propagating. The results indicate that wave absorption by the subway station and its reflection to the upper layers caused a gradual increase in acceleration toward the ground surface.

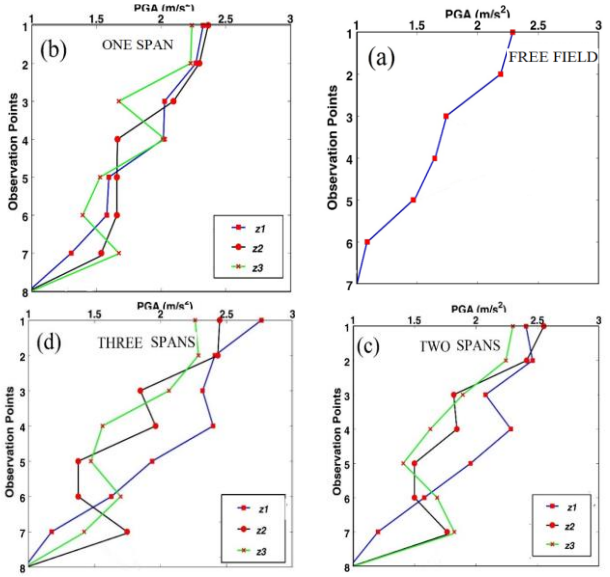

Fig. 10: Effect of the station width and its embedment, a) free-field, b) one span, c) two spans, d) three spans.

5.3 Effect of the subway station on the peak relative lateral displacement (PRLD)

This section compares the effect of cross-section dimensions and embedment of the subway on the peak relative lateral displacement (PRLD). The PRLD, here, is defined as a difference between the peak horizontal displacement time history at the top and bottom of the underground structure. As can be seen in figure 11, with increasing the subway embedment, the PRLD decreases. It shows an increase when the subway dimension increases. The highest relative displacement was recorded in 3-spans and at the z1 level with 7.77 mm. All models illustrate small differences in the relative displacement when the embedment of the structure goes from the level z2 to z3. It can be concluded that by increasing the embedment of the subway when subjected to near-fault earthquakes, the effects of the PRLD ratio can be ignored. Therefore, among the studied parameters, increasing the cross-section dimensions of the underground structure can be considered a highly effective factor.

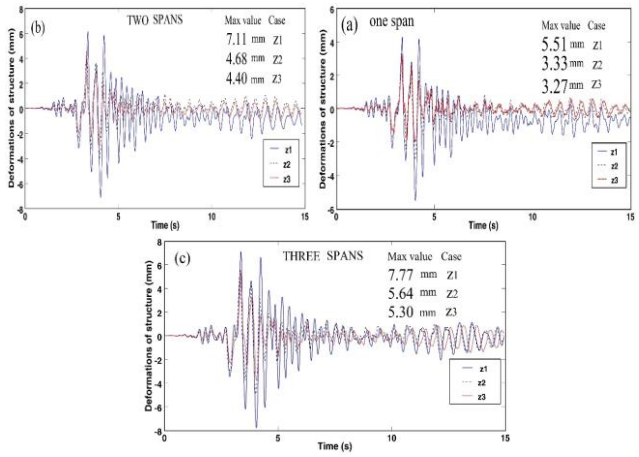

Fig. 11: Effect of the subway station on the PRLD, a) one span, b) two spans, c) three spans.

6. Effect of the far-fault ground motions

Figure 12 illustrates the PGA values of the observation points on the ground surface for all models when subjected to the far field earthquake. The peak responses occurring near points 1 to 9 are located in similar positions reported in the previous section, showing the significant role of subway presence in scattering of the seismic wave and amplifying the PGA. While for the embedment at z2 and z3 in the same positions compared to the free-field model, especially near the subway, the PGA shows de-amplification and a tendency to be less pronounced.

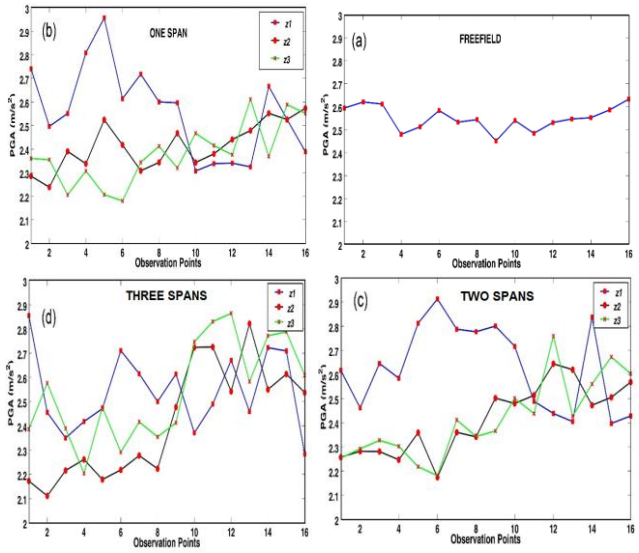

Fig. 12: Effect of the cross-section and embedment of the subway subjected to far-fault ground motions, a) free-field, b) one span, c) two spans, d) three spans.

Figure 13 illustrates the effect of cross-section dimensions and embedment of the subway on the peak relative lateral displacement (PRLD) subjected to far-fault ground motion. PRLD indicates an increase and a decrease with deepening the subway embedment and increasing its cross-section dimensions' size, respectively. The highest relative displacement was recorded in 3-spans and at z1 level with 8.01 mm. By increasing the cross-section of the structure from one span to three spans, the PRLD ratio shows 1.6 times of increase, highlighting the importance of subway dimensions on the PRLD ratio.

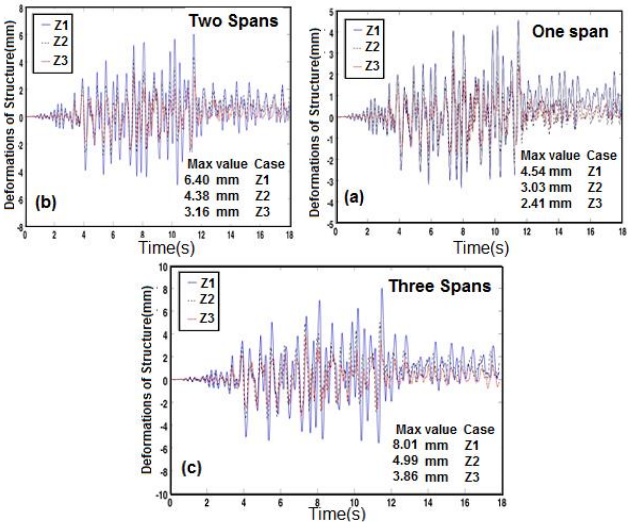

Fig. 13: Effect of the subway station on the PRLD subjected to far-fault ground motions, a) one span, b) two spans, c) three spans

7. Effect of the input motions on the seismic response

Figure 14 indicates the spectral acceleration ratios of different ground surface positions at 5% damping. The spectral ratio is defined as the ratio of the response spectra of the surface accelerations between the response spectra of the surface accelerations in the far-fault earthquake and the near-fault earthquake. The results indicate that the significant effects of input motion depend on the periods. The spectral ratio close to 0.5 for periods greater than 1.5 s indicates a minor influence of surface positions and embedment of the underground station on the response spectra. The amplification is more prominent when it depends on the positions and the subway depth, the periods are less than 0.5 s. The spectral ratio less than 1 for periods greater than 1 s shows a significant effect of the near-fault earthquake on response spectra. The amplification/ de-amplification effect is more prominent when independent from the surface positions, the periods are greater than 0.5 s. With increasing distance from the subway, the amplification effect gradually decreases.

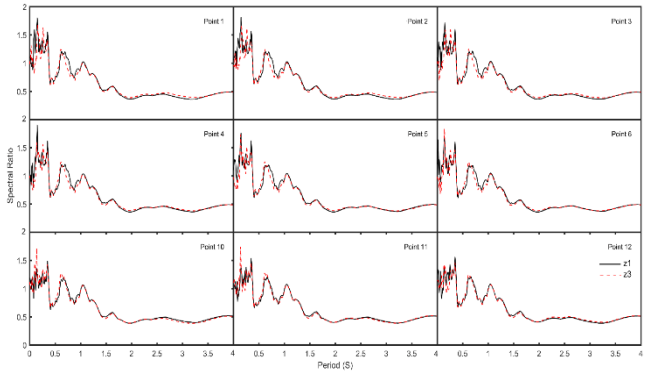

Fig. 14: Spectral acceleration ratios for the far-fault earthquake to the near-fault earthquake.

As seen in figure 15, the maximum spectral ratio of 1.9 at point 4 at depth Z1 and the maximum value of 1.83 at point 6 at depth Z3 are observed. At points (1-6), the highest spectral ratios appear near the period of 0.15 s at depth Z1. While at points (10-12), an amplification appears around a period equal to 0.35 s at the same depth. At depth Z3, at all points, the highest spectral ratios are near the period of 0.15 s. In addition, a rapid change in the spectral ratio is observed from points 3 to 5, which is caused by the edge of the subway station. The results in this section indicate various amplification or de-amplification at each frequency for different surface positions. Therefore, the characteristics of the input ground motion are key parameters affecting the ground surface response with the presence of a subway.

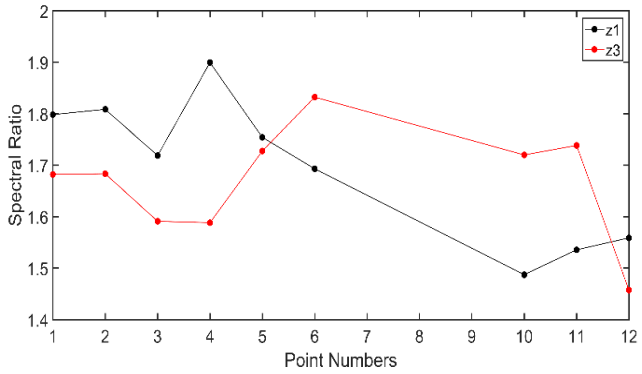

Fig. 15: Maximum spectral accelerations ratio for the embedment Z1 and Z2.

Figure 16 investigates the effect of input motion on the PRLD ratio (far-fault PRLD/near-fault PRLD). From the results, far-fault earthquakes cause a lower PRLD than near-fault earthquakes. Regardless of the size of the subway, its presence at depth Z3 considerably shows this effect. While for depth Z1, the size of the subway affects the PRLD ratio in different ways.

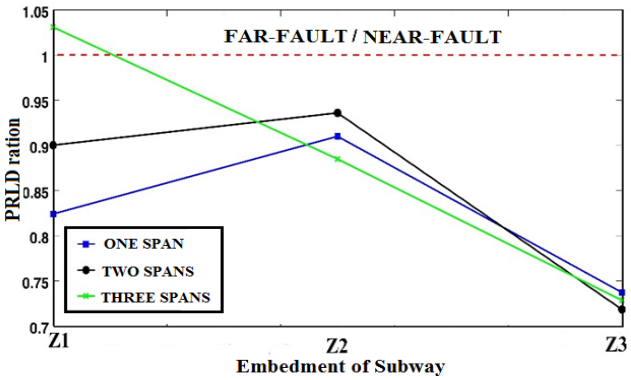

Fig. 16: Ratio of Far-fault and Near-fault ground motion and its effect on the PRLD ratio.

8. Effect of the interaction between two-subway station on the ground motion

In this section, the effect of the two subway stations compared to one subway station on the ground response is discussed. Figure 17 illustrates the geometry of the two-subway stations, where their distance from each other is W. W takes on different values, including 0.5B, B, 1.5B, and 2B. PGA recorded in the soil layers and on the ground, surfaces are shown in Figures 18 and 19 for the near-fault and far-fault earthquakes, respectively. Both figures indicate that the presence of the double subway station does not have a considerable effect on amplifying the PGA and the pattern of PGA amplification.

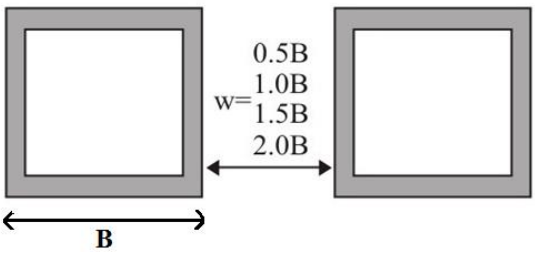

Fig. 17: Schematic double subway station in four distances 0.5B, B, 1.5B, and 2B.

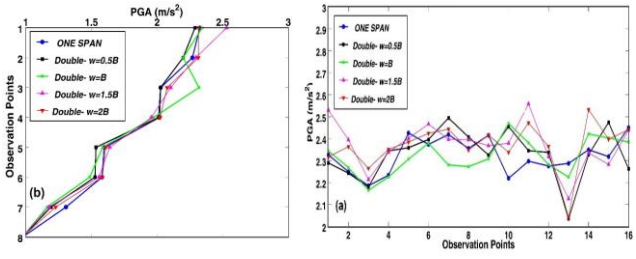

Fig. 18: Effect of the double subway station on the PGA subjected to near-fault ground motion, a) surface ground, b) soil layers.

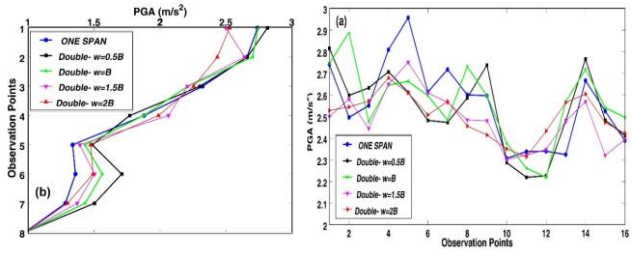

Fig. 19: Effect of the double subway station on the PGA subjected to far-fault ground motion, a) ground surface, b) soil layers.

9. conclusion

This study investigated the effect of subway station characteristics on the scattering of seismic waves. The input motion, the embedment of the structure, double station, a novel nonlinear cyclic model, and the underground station dimensions were considered. The conclusions below were obtained from the outcomes of the present study:

The amplification effect of the subway station on the ground motions was evaluated. Since the dynamic effects of such underground structures are prominent, the seismic design for structures on ground surface should consider the presence of subway station.

A significant amplification/de-amplification of the peak ground acceleration was observed with the decreasing/increasing embedment of the underground structure. More importantly, with the increasing embedment of the subway, the peak relative lateral displacement decreased.

The numerical results reveal that a significant influence appears when a subway station dimension is increased. A 1.6 times increase in the relative displacement indicated and a 1.2 times increase in the surface ground acceleration indicated that the cross-section of the subway has a significant influence on the amplification ratio and scattering on the wave.

The results indicated that each frequency may result in various amplification or de-amplification effects at different locations on the ground surface. The amplification effect is more significant when periods less than 0.5 s, depending on the positions and the subway depth. A spectral ratio less than 1 for periods greater than 1 s indicates a significant effect of the near-fault earthquake on the response spectra.

References

[1] Iida H, Hiroto T, Yoshida N, Iwafuji M. (1996) Damage to Daikai subway station. *Soils Found* 36:283–300.

[2] Power M, Rosidi D, Kaneshiro J, Gilstrap S, Chiou S. (1998) Summary and evaluation of procedures for the seismic design of tunnels. Final Report Task.

[3] Chen G, Wang Z, Zuo X, Du X, Gao H. (2013) Shaking table test on the seismic failure characteristics of a subway station structure on liquefiable ground. Earthq Eng *Struct Dyn* 42:1489–507.

[4] Sun Q, Dias D, Guo X, Li P. (2019) Numerical study on the effect of a subway station on the surface ground motion. *Computers and Geotechnics*;111: 243–254.

[5] Ma C, Lu D, Du X, Qi C, Zhang X. (2019) Structural components functionalities and failure mechanism of rectangular underground structures during earthquakes. *Soil Dyn Earthq Eng* 119: 265–280.

[6] Isari M, Damadipour M, Taghavi Ghalesari A, Razavi SK& Tarinejad R (2021). Modal Identification of a Soil-subway System with Emphasis on Scattering of Seismic Waves Induced by Uniform and Non-Uniform Support Excitations, *Journal of Earthquake Engineering*, DOI: 10.1080/13632469.2021.1927890.

[7] Jing-Ming W, Litehiser JJ. (1985) The distribution of earthquake damage to underground facilities during the 1976 Tang-Shan earthquake. *Earthq Spectra* 1:741–57.

[8] Sharma S, Judd WR. (1991) Underground opening damage from earthquakes. Eng Geol 30:263–76.

[9] Xu Z, Du X, Xu C, Hao H, Bi K.(2019). Numerical research on seismic response characteristics of shallow buried rectangular underground structure. *Soil Dyn Earthq* Eng;116: 242–252.

[10] Xu Z, Du X, Xu C, Jiang J, Han R. (2019). Simplified equivalent static methods for seismic analysis of shallow buried rectangular underground structures. *Soil Dyn Earthq* Eng;121: 1-11.

[11] Panji M., Kamalian M., Marnani J.A., and Jafari, M.K. (2013). Transient analysis of wave propagation problems by half-plane BEM. *Geophysical Journal International*, **194**, 1849-1865.

[12] Panji M., Kamalian M., Asgari Marnani J., and Jafari, M.K. (2014). Antiplane seismic response from semi-sine shaped valley above embedded truncated circular cavity: a time-domain half-plane BEM. *International Journal of Civil Engineering, Transaction B: Geotechnical Engineering*, **12**, 193-206.

[13] Alielahi H., Kamalian M., Asgari Marnani J., Jafari M.K., and Panji, M. (2013). Applying a time-domain boundary element method for study of seismic ground response in the vicinity of embedded cylindrical cavity. *Int. J. Civil Eng*., **11**, 45-54.

[14] Alielahi H., Kamalian M., and Adampira M. (2015). Seismic ground amplification by unlined tunnels subjected to vertically propagating SV and P waves using BEM. *Soil Dynamics and Earthquake Engineering*, **71**, 63-79.

[15] Alielahi H. and Adampira M. (2016). Seismic effects of two-dimensional subsurface cavity on the ground motion by BEM: amplification patterns and engineering applications. *International Journal of Civil Engineering*, **14**, 233-251.

[16] Zhuang H, Yang J, Chen S, Dong, Z, Chen G. (2021) Statistical numerical method for determining seismic performance and fragility of shallow-buried underground structure, Tunneling and Underground Space Technology,

Volume 1161014090, ISSN 0886-7798, https://doi.org/10.1016/j.tust.2021.104090.

[17] Zhu T, Wang R, Zhang J-M. (2021) Effect of nearby ground structures on the seismic response of underground structures in saturated sand, Soil Dynamics and Earthquake Engineering, Volume 146, 2021, 106756, ISSN 0267-7261, https://doi.org/10.1016/j.soildyn.106756.

[18] Ma C, Lu D, Gao H, Du X, Qi C (2021) Seismic performance improvement of underground frame structures by changing connection type between sidewalls and slab, *Soil Dynamics and Earthquake Engineering*, Volume 149, 106851 ISSN0267-7261, https://doi.org/10.1016/j.soildyn.2021.106851.

[19] Gao Z, Zhao M, Du X, M. El Naggar H, Wang J, (2021) Seismic analysis of underground structures employing extended response spectrum method, Tunnelling and Underground Space Technology, Volume 116,2021,104089, ISSN 0886 7798, https://doi.org/10.1016/j.tust.2021.104089.

[20] Ding, X, Zhang, Y, Wu, Q, Chen, Z, Wang, C, (2021) Shaking table tests on the seismic responses of underground structures in coral sand, Tunnelling and Underground Space Technology, Volume 109,2021,103775, ISSN 0886-7798, https://doi.org/10.1016/j.tust.2020.103775.

[21] Zhou, H, Cong, P, Wang, X, Wang, Y, Dai, H, Yu, S, Du, J. (2021) Global response of underground structures subjected to ground shock with consideration of rise time, *Soil Dynamics and Earthquake Engineering*, Volume 143, 106624 ISSN 0267-7261, https://doi.org/10.1016/j.soildyn.2021.106624.

[22] Zhu, T, Wang, R, Zhang, J-M. (2021) Evaluation of various seismic response analysis methods for underground structures in saturated sand, Tunnelling and Underground Space Technology, Volume 110,103803, ISSN 0886-7798, https://doi.org/10.1016/j.tust.2020.103803.

[23] Wichtmann, T., & Triantafyllidis, T. (2009). Influence of the grain-size distribution curve of quartz sand on the small strain shear modulus G max. *Journal of geotechnical and geoenvironmental engineering*, 135(10), 1404-1418.

[24] Payan, M., Khoshghalb, A., Senetakis, K., & Khalili, N. (2016). Effect of particle shape and validity of Gmax models for sand: A critical review and a new expression. *Computers and Geotechnics*, 72, 28-41.

[25] Payan, M., Senetakis, K., Khoshghalb, A., & Khalili, N. (2017). Characterization of the small-strain dynamic behavior of silty sands; contribution of silica non-plastic fines content. *Soil Dynamics and Earthquake Engineering*, 102, 232-240.

[26] Menq, F. Y. (2003). Dynamic properties of sandy and gravelly soils. The University of Texas at Austin.

[27] Wichtmann, T., & Triantafyllidis, T. (2013). Effect of uniformity coefficient on G/G max and damping ratio of uniform to well-graded quartz sands. *Journal of geotechnical and geoenvironmental engineering*, 139(1), 59-72.

[28] Wichtmann, T., Hernández, M. N., & Triantafyllidis, T. (2015). On the influence of a non-cohesive fines content on small strain stiffness, modulus degradation and damping of quartz sand. *Soil Dynamics and Earthquake Engineering*, 69, 103-114.

[29] Yniesta, S., Brandenberg, S.J., and Shafiee A. (2017) "ARCS: One-dimensional Non-linear Model for Ground Response Analysis" *Soil Dynamics and Earthquake Engineering*, 102, 75-85.

[30] Itasca. 2011. *Fast Lagrangian analysis of continua in 3 dimensions, user's guide. FLAC3D V5.0. Minneapolis*: Itasca Consulting Group

[31] Razavi, S.K., Hajialilue-Bonab, M. and Pak, A., 2021. Design of a Plastic Concrete Cutoff Wall as a Remediation Plan for an Earth-Fill Dam Subjected to an Internal Erosion. *International Journal of Geomechanics*, 21(5), p.04021061.